PHYSICAL REVIEW A **91**, 031403(R) (2015)

Understanding the modulation mechanism in resonance-enhanced multiphoton probing of molecular dynamics

Markus Koch,[1,2,*] Thomas J. A. Wolf,[1] and Markus Gühr[1]

[1]*Stanford PULSE Institute, SLAC National Accelerator Laboratory, Menlo Park, California 94025, USA*

[2]*Institute of Experimental Physics, Graz University of Technology, Petersgasse 16, A-8010 Graz, Austria*

(Received 29 August 2014; published 30 March 2015)

Time-resolved spectroscopy on isolated molecules gives fundamental insight into the conversion of light energy to other degrees of freedom. Probing of the photoinduced dynamics can be accomplished by ionization, via a single-photon or multiphoton transition. In this Rapid Communication we directly contrast transient spectra on the molecule perylene obtained with multiphoton ionization (MPI) to single-photon ionization (SPI). The photoinduced nuclear geometry relaxation modulates the MPI transient with a decay time constant of 0.9 ± 0.2 ps. In contrast, the SPI transient completely lacks any indication for relaxation. We attribute this difference to a change in resonance enhancement of the MPI probe as the molecular geometry changes. Our results underline the importance of a detailed knowledge about these resonances for a proper interpretation of transient signals of molecular dynamics subject to nuclear and electronic relaxation effects. At the same time, the direct comparison to SPI directly demonstrates the higher sensitivity of resonance-enhanced MPI as a probe in time-resolved dynamical studies.

DOI: 10.1103/PhysRevA.91.031403 PACS number(s): 33.20.Xx, 33.60.+q, 82.53.Hn

The conversion of photon energy into other forms of energy is often happening with high selectivity and efficiency [1]. Time-resolved photoelectron (PE) and photoion (PI) spectroscopy have proven to be important tools for the investigation of photoinduced relaxation processes in isolated molecules [2–4], since their observables can be simulated from theoretical investigations with high accuracy and thus directly compared [5,6]. The molecular relaxation generally leads to an increased ionization potential [7]. In order to detect the dynamics via a single-photon ionization (SPI) scheme, increased probe photon energies in the vacuum ultraviolet (VUV) [8–13] have been recently applied. Experimentally less demanding and therefore widely used is multiphoton ionization (MPI) [2,4,14,15], as shown for metal carbonyls [16,17] or nucleobases [18–21]. As pointed out before, the transient MPI signal can be enhanced by resonant excited molecular states [14–17]. However, the role that the resonances play in actively shaping the observable transient in a pump–MPI-probe experiment has not been investigated. In this paper, we fill this gap by comparing SPI and MPI for identical molecules and excitation conditions finding stark differences in the transient spectra obtained by the two processes. The comparison of the SPI and MPI transients together with laser intensity characteristics directly reveals the active influence of the resonances on the observable in MPI probing.

Figure 1 shows a sketch of the important processes in time-resolved PE and PI spectroscopy. An excitation (pump) laser pulse promotes the molecule from the ground state S_0 into an electronically excited state S_1. A second ultrashort laser (probe) pulse interacts with the excited molecule after a controlled delay. It can ionize the excited molecules either via SPI or MPI. In order to ionize the molecule via SPI, the photon energy has to be larger than the excited-state ionization potential [7]. For this case, the probe laser field projects the excited-state nuclear wave packet onto one or more electronic continua. The resulting PI and PE spectra are measured as a function of pump-probe pulse delay. The ionization yield and the PE energy are modulated by the molecular dynamics if the SPI step is sensitive to nuclear and/or electronic relaxation. Alternatively to SPI, the ionization energy can be overcome by several photons in MPI schemes [2,14–21]. Here relaxation processes are generally observed as transient changes of ion (fragment) yields. As shown in Fig. 1, the MPI signal can be enhanced by intermediate resonant states.

For our systematic study, we choose the polycyclic aromatic hydrocarbon perylene. It presents a conceptually simple case performing *only* nuclear dynamics after photoexcitation with negligible internal conversion and intersystem crossing [22,23] (excited population thus stays in the S_1 state in Fig. 1). We will show that for the resonantly enhanced MPI, the transient ion signal exhibits a transient signal decay of 0.9 ± 0.2 ps. In contrast, the SPI shows absolutely no modulation in the PE energy. In the following, we will discuss the differences in the transient signals of the two schemes in combination with additional information about the MPI process from laser intensity scans and from time-dependent density-functional theory (TDDFT) calculations.

The experiments are carried out with a recently developed time-resolved PE and PI spectrometer [24]. A molecular beam of perylene (Sigma Aldrich, purity greater than 99.5%) is introduced into the interaction region by a resistively heated capillary oven [25].

Following 400-nm pump excitation, the molecular dynamics is probed after a time delay either using SPI or MPI. For use in SPI, VUV probe pulses are obtained from high-order-harmonic generation in Ar gas [26]. The ninth harmonic (89 nm, 14-eV photon energy) is isolated from the high-harmonic continuum by using the bandpass characteristics of an indium metal filter [24]. The isolated ninth-harmonic pulse duration is 35 ± 8 fs and its spectral width is 190 ± 60 meV. For MPI the 800-nm laser fundamental is used. The pump-probe time resolution of 65 ± 10 fs is deduced from the rise

*Corresponding author: markus.koch@tugraz.at

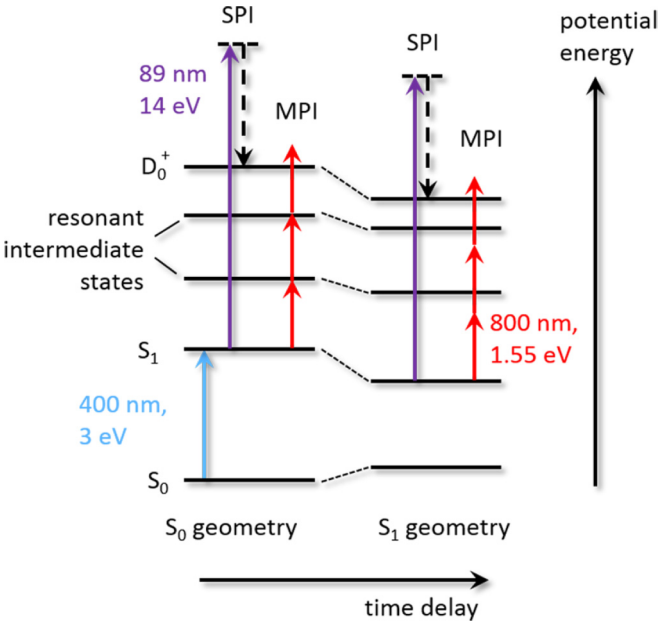

FIG. 1. (Color online) Sketch of the electronic states of perylene and excitation-ionization schemes. Shown are the ground state S_0, the first excited state S_1, resonant intermediate states, and the lowest ionic state D_0^+ for S_0 and S_1 minimum geometries. After 400-nm excitation the molecule is either ionized by SPI with a single 89-nm VUV photon or via 800-nm MPI. During vibrational relaxation in the excited state the ionization potential (S_1-D_0^+ distance) remains nearly constant, while the energy distance to states that lead to resonance enhancement of the MPI probe increases.

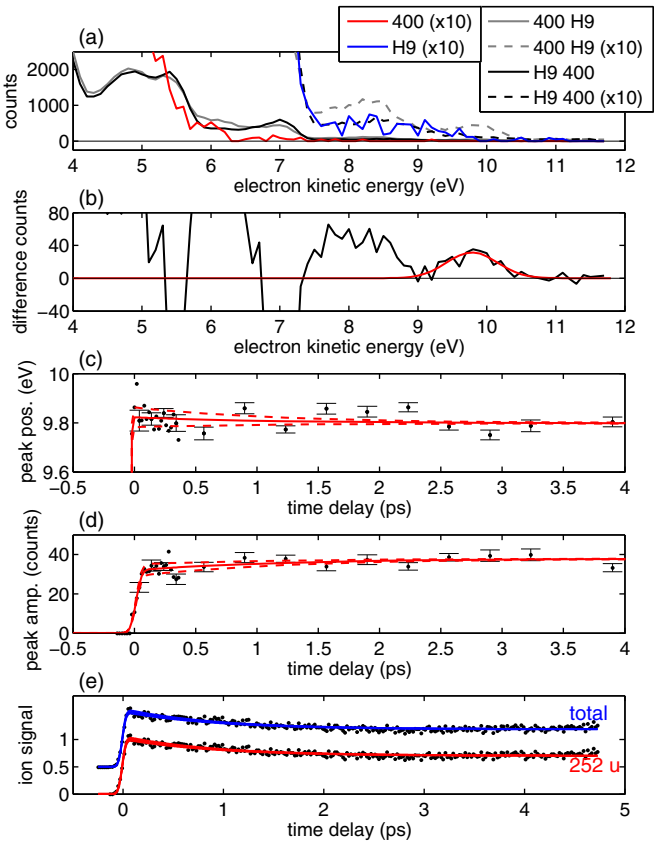

FIG. 2. (Color online) Comparison of H9 (89-nm) SPI probing with 800-nm MPI probing for perylene pump-probe photoionization. (a) PE spectra obtained with the 400-nm and H9 pump-probe spectrum (gray), H9 and 400-nm probe-pump signal (black), 400-nm pump pulse only (red), and H9 probe only (blue). Traces are additionally shown with a magnification of 10 for better visibility. (b) Difference spectrum obtained as the pump-probe spectrum minus the probe-pump signal (black) together with a Gaussian fit of the PE peak at 9.8 eV (red). (c) Position of the 9.8-eV PE peak as obtained from the Gaussian fit as a function of the pump-probe time delay. A fit with the product of an error function and an exponential term with variable amplitude (red curve) [31] (see also [32], Table 2) reveals a negligible PE signal shift of $-0.2 \pm 0.5\%$. The red dashed lines mark the 95% confidence interval of the exponential term amplitude. (d) Same as in (c) for the PE peak amplitude. The fit gives a $15 \pm 10\%$ increase with a 1.2-ps time constant. (e) Transient PI signals for 800-nm MPI probing observed at the perylene parent ion mass at 252 u (red curve) and for the total ion yield (blue curve, vertically offset by 0.5). Fits to the same function as in (c) and (d) reveal decays of $32 \pm 3\%$ (252 u) and $34 \pm 3\%$ (total ion yield), both with a 0.9 ± 0.2 ps time constant (see [32], Table 2).

time in the pump-probe spectra and applies for MPI and SPI [24].

For VUV SPI we detect PE spectra with a magnetic bottle electron time-of-flight spectrometer and deduce molecular dynamics from a transient change of the PE kinetic energy. We choose a pump pulse intensity of $\sim 4 \times 10^{10}$ W/cm^2 to excite about 17% of the perylene molecules to the S_1 state [24]. Although PEs are produced by the 400-nm pulse alone due to some small multiphoton ionization probability, excitations to states higher than S_1 are negligible for the pump-probe signal, as no PE bands are detected above 10 eV [Fig. 2(a)].

For MPI we deduce the molecular dynamics from a transient change of the ion yield. Here we do not show MPI PE spectra since their interpretation requires the decomposition of electrons emerging from several ionic continua. We therefore operate the time-of-flight spectrometer in ion mode. Sufficiently low laser intensities are chosen to obtain negligible signals from the pump or probe laser alone, as compared to the pump-probe signal.

In addition to our experimental results, we perform geometry optimizations and excitation energy calculations on the (TD)DFT level of theory as implemented in the GAMESS-US program package [27]. The ground-state geometry is optimized using B3LYP/def2-SVP. Excited-state energy and geometry optimization calculations are carried out with TDB3LYP/MCP/NOSeC-V-DZP. Since both S_0 and S_1 minima exhibited D_{2h} symmetry, all calculations are carried out in D_{2h}. Ionization potentials are calculated with OVGF/QZVP as implemented in GAUSSIAN09 [28].

A comparison of SPI and MPI probing for transient pump-probe spectroscopy of perylene is shown in Fig. 2. The SPI PE spectrum of unexcited perylene obtained with harmonic number 9 (H9) (14 eV and 89 nm) consists of five distinct PE bands in the kinetic energy range of 0–7 eV and fits the literature data [24,29]. Our resolution suffices to clearly separate the lowest-lying ionic state continuum (7-eV kinetic energy) from all the other continua. The lowest ionic states

(cf. Fig. 1) give rise to the two photoelectron peaks centered at 5.0 and 6.8 eV [30] [Fig. 2(a)]. A preceding 400-nm (3.1-eV) pump pulse excites a fraction of the molecules to the S_1 ($1B_{2u}$) state and its ionization leads to the appearance of two new PE peaks at 8.1 and 9.8 eV in the PE spectrum [Fig. 2(a)], reflecting the excess potential energy. The difference of the pump-probe (400 nm and H9) (gray) spectrum and the time-reversed probe-pump signal (H9 and 400 nm) (black), serving as the background correction, is depicted in Fig. 2(b). It clearly shows the two excited-state PE peaks. The strong modulations of the difference signal below 8 eV reflect a decreased ionization yield from S_0 overlapping with the emerging PE signal due to ionization from S_1 [24]. We fit the PE signal corresponding to ionization from S_1 to the ionic ground state $D_0{}^+$ at 9.8 eV by a Gaussian function [red curve in Fig. 2(b)]. Figures 2(c) and 2(d) show the peak position and amplitude, respectively, of the Gaussian fit as a function of pump-probe time delay. We fit the data by the product of an error function and an exponential term with variable amplitude (red) [31] (see also [32], Table 2). The 9.8-eV PE peak position shows essentially no delay dependence. Considering the 95% confidence interval of the exponential decay amplitude (red dashed lines) we find a negligible PE signal shift of $-0.2 \pm 0.5\%$. Note that Fig. 2(c) shows the peak positions within a narrow range of 0.4 eV. From this time-delay-independent character we conclude that either no relaxation takes place in the S_1 state or the ionization potential from S_1 to $D_0{}^+$ is constant within an experimental uncertainty of less than 1% during relaxation from S_0 to S_1 geometry.

The transient position of the 9.8-eV PE peak obtained with SPI is now compared to transient 800-nm MPI signals, which are shown in Fig. 2(e) for detection of the unfragmented parent ion ($C_{20}H_{12}{}^+$ at 252 u) (red curve) and the total ion yield (blue curve). Surprisingly, both transient PI signals show a strong signature for molecular relaxation. After the fast increase around zero delay, which represents the pump-probe cross correlation [24], we observe exponential signal decays by $32 \pm 3\%$ (parent ion) and $34 \pm 3\%$ (total ion yield), both with a time constant of 0.9 ± 0.2 ps (see [32], Table 2). This is in good agreement with time scales for intramolecular vibrational redistribution reported in the literature [33]. In addition to the parent ion, we observe the ion fragments $C_{20}H_{10}{}^+$ (250 u, 5% of the parent yield), $C_{20}H_8{}^+$ (248 u, 1%), $C_{19}H_8{}^+$ (236 u, 7%), and the doubly charged parent ion $C_{20}H_{12}{}^{2+}$ (126 u, 2%). These ions result from ionization to higher ionic continua and exhibit an exponential decay comparable to that of the parent and total ion yields. From the equivalence of all ion signal decays we conclude that fragmentation in the ionic ground state with increasing pump-probe delay, due to energy gain during relaxation in the S_1 state, does not take place. Hence, the transient parent ion signal [Fig. 2(e), red curve] corresponds to MPI to the ionic ground state $D_0{}^+$ and should therefore represent the same time dynamics as the SPI PE signal. Obviously, the decaying parent ion yield in MPI for increasing pump-probe delay is in strong contrast to the constant character of the SPI PE peak position [Fig. 2(c)]. From the unshifted PE peak in the SPI transient one would conclude that no molecular relaxation occurs and thus expect that the MPI transient ion yield would also be unmodulated.

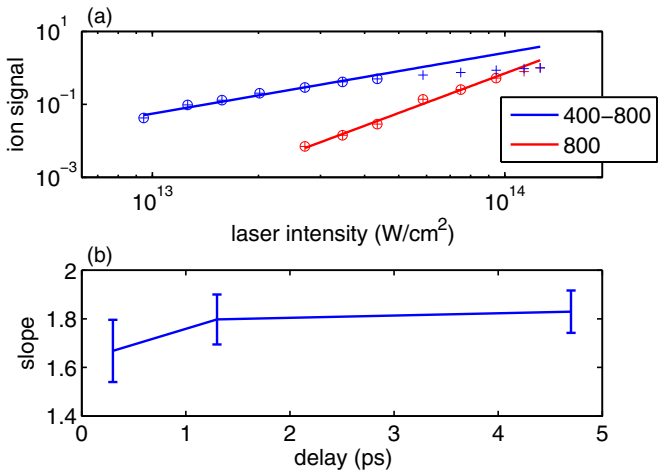

FIG. 3. (Color online) (a) Laser intensity scans for 800-nm (red) (252-u detection and slope equal to 3.60 ± 0.18), as well as 400- and 800-nm pump-probe MPI (blue) (252-u detection, time delay of 0.3 ps, and slope equal to 1.67 ± 0.13). Due to saturation of the process, the data points (crosses) for the highest laser intensities deviate from the expected linear dependence. Only encircled data points are included in the fit. (b) Slopes for 400- and 800-nm pump-probe MPI at different time delays.

To obtain a deeper insight into this discrepancy we determine the order of the MPI process. For MPI, the ion yield as a function of the laser intensity shows a linear dependence in a log-log plot and its slope is related to the order of the ionization process. Figure 3(a) presents the unfragmented parent ion yield as a function of the 800-nm laser intensity for MPI from the S_0 ground state (red) and for MPI from the S_1 excited state with the preceding 400-nm excitation (blue). Due to the vertical ionization potential of 7 eV of ground-state perylene [29], a process order of 5 is expected for 800-nm (1.55 eV) MPI. The observed order of 3.60 ± 0.18 demonstrates the presence of intermediate states, which lead to resonant enhancement of the ionization process. The noninteger value is due to intensity averaging over the focused laser beam [34,35]. With the preceding 400-nm (3.1 eV) pump excitation to the S_1 state we observe a process order of 1.67 ± 0.13. This reduction by a factor of 2 reflects the absorption of one 400-nm photon. It demonstrates the presence of resonant intermediate states also for MPI from S_1, which we will use in the following to explain the discrepancy of the transient SPI and MPI signals. To obtain insight into the transient behavior of these intermediate resonances, we measure the S_1 MPI process order for different pump-probe time delays [Fig. 3(b)]. Although the error bars overlap, the graph indicates an increase of the observed slopes from 1.67 ± 0.13 at 0.3-ps delay to 1.83 ± 0.09 at 4.7 ps.

Based on the resonant character of the MPI probe process, we are able to explain the origin of the dynamic modulation *purely based on experimental data*. The constant PE energy in the SPI transients can only result from a constant energy difference of the cationic ground state $D_0{}^+$ and S_1 along the nuclear relaxation coordinate. Thus, the modulation in the transient MPI signal must be a consequence of a different energy change related to the intermediate resonant state (or states). Indeed, the changing order as a function of delay also

supports this assignment. The decrease of the transient results from an intermediate state (or states) shift out of resonance with respect to the laser spectral center.

The amplitude of the SPI PE peak as a function of the delay is shown in Fig. 2(d). Unlike the constant peak position, the amplitude shows an increase of $15 \pm 10\%$ with a 1.2-ps time constant. This points towards an increase of the transition strength (Franck-Condon factor and/or dipole moment) between S_1 and $D_0{}^+$ during molecular relaxation from S_0 to S_1 geometry. The temporal behavior of the 8.1-eV PE peak shows the same transient trends in position and amplitude, albeit with increased noise presumably because of the mentioned modulations of the difference signal due to overlapping PE bands.

Although the experimental results are self-conclusive, we perform geometry optimizations and excitation energy calculations on the (TD)DFT level of theory to support our findings. Despite the uncertainties of the TDDFT calculations especially regarding states with strong Rydberg character close to the first ionization potential (IP), our calculations predict the presence and relative shift of intermediate resonances. We find an almost parallel decrease in potential energy of S_1 and of the $D_0{}^+$ for relaxation from the Franck-Condon region to the S_1 minimum nuclear geometry (see [32], Fig. 1 and Table 1). Over this path, the S_1-$D_0{}^+$ potential energy difference increases by only 50 meV. This is in agreement with our SPI data and the observed shift of the 9.8-eV PE peak by -20 ± 50 meV ($-0.2 \pm 0.5\%$), which is negligible with respect to the spectral width. Our calculations also predict the presence of intermediate states that lead to resonant enhancement of MPI from both the S_0 and S_1 states, in agreement with the observed MPI orders (Fig. 3). For MPI from S_0 (gerade symmetry) these are an ungerade state at 4.98 eV ($2B_{1u}$) and a gerade state at 6.36 eV ($2B_{1g}$) (see [32], Fig. 1 and Table 1). For MPI from S_1 (ungerade) two gerade states ($3B_{3g}$ and $4B_{3g}$) at 4.22 and 4.67 eV and five ungerade states ($5B_{1u}$, $5B_{2u}$, $6B_{2u}$, $6B_{1u}$, and $7B_{2u}$) in the range of 6.1–6.3 eV can lead to resonant enhancement. For these intermediate states the potential energy distance to S_1 depends much more on the molecular geometry than for the cationic ground state $D_0{}^+$. The energy gap to S_1 increases from S_0 to S_1 minimum geometry by 50 and 130 meV, respectively, for the two gerade states and by 130–330 meV for the five ungerade states. A comparison to the transform limited laser bandwidth of 70 meV shows that the magnitude of resonance enhancement decreases from the S_0 to the S_1 geometry. This is directly observable in our MPI measurements as a decrease in ion yield [Fig. 2(e)] and an increase of the process order [Fig. 3(b)] with progressing pump-probe delay.

Distinct resonance-enhanced ionization channels can be formulated for the two ionization schemes (800 and 400–800 nm) based on state symmetry considerations and Koopmans correlations. In the case of 800-nm ionization from the ground state (S_0 and $1A_g$), the energy of five photons (each 1.55 eV) is needed to overcome the first IP of 7 eV to the lowest cationic state [29]. The first step is a three-photon transition, since states of suitable energy and symmetry are missing for a single- or two-photon transition. The most probable candidate is the $2B_{1u}$ state at a calculated potential energy of 4.98 eV (see [32], Fig. 1 and Table 1). It exhibits the character of a highest occupied molecular orbital (HOMO)–lowest unoccupied molecular orbital (LUMO) +4 excitation. Absorption of a further photon leads to an energy region just below the IP where a plethora of states with suitable symmetry and character can be expected. From there the molecule can be ionized with an additional photon to the lowest cationic state $D_0{}^+$, which is characterized by removal of an electron from the HOMO.

For 400–800 nm two-color ionization, a possible ionization channel leads in a first step to the lowest excited state ($1B_{2u}$, HOMO-LUMO excitation) upon absorption of a 400-nm photon. By absorption of one 800-nm photon each, the molecule is most likely further excited to the $4B_{3g}$ state (4.67 eV), which exhibits at least partly the character of a HOMO-LUMO+1 excitation, and to the energy region just below the IP. From there single-photon ionization is possible.

In summary, we presented a systematic comparison of SPI and resonant MPI to study photoinduced dynamics in perylene, a conceptually simple molecule only exhibiting ultrafast intermolecular vibrational relaxation after photoexcitation into the S_1 state. The two probing schemes, which are widely used in time-resolved experiments [2,8–21], exhibit strong differences in their sensitivity to this relaxation processes. While photoelectron spectroscopy based on SPI does not show any modulation with pump-probe delay, the MPI shows a clear signal decay within 1 ps. We established the presence of intermediate resonances for the MPI probe step via laser intensity scans. The time-dependent SPI photoelectron spectroscopy indicates a constant energy difference of the S_1 and D_0 states over the relaxation path and in addition a negligible decay of population into other product states, as anticipated due to the high fluorescence yield of the molecule [33]. We therefore concluded that the decay observed in MPI must necessarily result from the resonances shifting as the molecule relaxes. We qualitatively supported this experimental argument by TDDFT simulations. This finding is generally important for the interpretation of ultrafast MPI transients in molecules with more complex relaxation pathways since signatures arising from intramolecular vibrational relaxation cannot be distinguished from signatures of non-Born-Oppenheimer processes within the experimental method. The distinction can only be made with the help of quantitatively correct results from quantum chemistry. High-level quantum chemical calculations are needed even to interpret results from SPI investigation of non-Born-Oppenheimer dynamics. The requirements for theory in the MPI case has to be even higher since the calculation of highly excited neutral states necessarily requires a higher-level treatment of electron correlation to predict acceptable energy differences. We therefore regard single-photon probing a better method for a systematic investigation of underlying molecular dynamics. Although high-harmonic sources have only been used on conceptually simple molecules [8–13] so far, application of SPI on more complex systems such as nucleobases, base pairs, and base-pair models [36] will be possible.

We thank Emily Sistrunk and Jakob Grilj for support with the experimental setup and Todd Martinez for valuable discussions. This work was supported by the AMOS program within the Chemical Sciences, Geosciences, and Biosciences Division of the Office of Basic Energy Sciences, Office of Science, U.S. Department of Energy. M.G. acknowledges funding via the Office of Science Early Career Research Program through

the Office of Basic Energy Sciences, U.S. Department of Energy. M.K. would like to acknowledge support by the Austrian Science Fund (FWF, Erwin Schrödinger Fellowship Grant No. J 3299-N20). T.J.A.W. thanks the German National Academy of Sciences Leopoldina for a fellowship (Grant No. LPDS2013-14).

[1] W. Domcke, D. R. Yarkony, and H. Köppel, *Conical Intersections: Theory, Computation and Experiment* (World Scientific, Singapore, 2011).

[2] A. Stolow and J. G. Underwood, Time-resolved photoelectron spectroscopy of nonadiabatic dynamics in polyatomic molecules, Adv. Chem. Phys. **139**, 497 (2008).

[3] A. Stolow, A. E. Bragg, and D. M. Neumark, Femtosecond time-resolved photoelectron spectroscopy, Chem. Rev. **104**, 1719 (2004).

[4] R. J. Levis and M. J. DeWitt, Photoexcitation, ionization, and dissociation of molecules using intense near-infrared radiation of femtosecond duration, J. Phys. Chem. A **103**, 6493 (1999).

[5] H. R. Hudock *et al.*, Ab initio molecular dynamics and time-resolved photoelectron spectroscopy of electronically excited uracil and thymine, J. Phys. Chem. A **111**, 8500 (2007).

[6] T. J. A. Wolf *et al.*, Hexamethylcyclopentadiene: Time-resolved photoelectron spectroscopy and ab initio multiple spawning simulations, Phys. Chem. Chem. Phys. **16**, 11770 (2014).

[7] M. Barbatti and S. Ullrich, Ionization potentials of adenine along the internal conversion pathways, Phys. Chem. Chem. Phys. **13**, 15492 (2011).

[8] L. Nugent-Glandorf *et al.*, Ultrafast time-resolved soft x-ray photoelectron spectroscopy of dissociating Br_2, Phys. Rev. Lett. **87**, 193002 (2001).

[9] D. Strasser, F. Goulay, and S. R. Leone, Transient photoelectron spectroscopy of the dissociative $Br_2(^1\Pi_u)$ state, J. Chem. Phys. **127**, 184305 (2007).

[10] P. Wernet *et al.*, Real-time evolution of the valence electronic structure in a dissociating molecule, Phys. Rev. Lett. **103**, 013001 (2009).

[11] H. Tao *et al.*, Ultrafast internal conversion in ethylene. I. The excited state lifetime, J. Chem. Phys. **134**, 244306 (2011).

[12] T. K. Allison *et al.*, Ultrafast internal conversion in ethylene. II. Mechanisms and pathways for quenching and hydrogen elimination, J. Chem. Phys. **136**, 124317 (2012).

[13] A. Makida *et al.*, Ultrafast relaxation dynamics in trans-1,3-butadiene studied by time-resolved photoelectron spectroscopy with high harmonic pulses, J. Phys. Chem. Lett. **5**, 1760 (2014).

[14] I. Wilkinson *et al.*, Excited state dynamics in SO_2. I. Bound state relaxation studied by time-resolved photoelectron-photoion coincidence spectroscopy, J. Chem. Phys. **140**, 204301 (2014).

[15] C. Okabe *et al.*, Ultrafast excited-state dynamics in photochromic N-salicylideneaniline studied by femtosecond time-resolved REMPI spectroscopy, J. Chem. Phys. **121**, 9436 (2004).

[16] S. A. Trushin, W. Fuß, and W. E. Schmid, Conical intersections, pseudorotation and coherent oscillations in ultrafast photodissociation of group-6 metal hexacarbonyls, Chem. Phys. **259**, 313 (2000).

[17] S. A. Trushin, W. Fuss, W. E. Schmid, and K. L. Kompa, Femtosecond dynamics and vibrational coherence in gas-phase ultraviolet photodecomposition of $Cr(CO)_6$, J. Phys. Chem. A **102**, 4129 (1998).

[18] S. Matsika, M. Spanner, M. Kotur, and T. C. Weinacht, Ultrafast relaxation dynamics of uracil probed via strong field dissociative ionization, J. Phys. Chem. A **117**, 12796 (2013).

[19] H. Kang *et al.*, Intrinsic lifetimes of the excited state of DNA and RNA bases, J. Am. Chem. Soc. **124**, 12958 (2002).

[20] C. Canuel *et al.*, Excited states dynamics of DNA and RNA bases: Characterization of a stepwise deactivation pathway in the gas phase, J. Chem. Phys. **122**, 074316 (2005).

[21] J. González-Vazquez, L. González, E. Samoylova, and T. Schultz, Thymine relaxation after UV irradiation: The role of tautomerization and $\pi\sigma^*$ states, Phys. Chem. Chem. Phys. **11**, 3927 (2009).

[22] B. Fourmann *et al.*, Fluorescence spectra and intramolecular vibrational redistribution in jet-cooled perylene, Chem. Phys. **92**, 25 (1985).

[23] M. Sonnenschein, A. Amirav, and J. Jortner, Absolute fluorescence quantum yields of large molecules in supersonic expansions, J. Phys. Chem. **88**, 4214 (1984).

[24] M. Koch *et al.*, Femtosecond photoelectron and photoion spectrometer with vacuum ultraviolet probe pulses, J. Electron Spectrosc. Relat. Phenom. **197**, 22 (2014).

[25] B. K. McFarland *et al.*, Experimental strategies for optical pump–soft x-ray probe experiments at the LCLS, J. Phys. Conf. Ser. **488**, 012015 (2014).

[26] J. Grilj, E. Sistrunk, M. Koch, and M. Gühr, A beamline for time-resolved extreme ultraviolet and soft x-ray spectroscopy, J. Anal. Bioanal. Tech. **S12**, 005 (2014).

[27] M. W. Schmidt *et al.*, General atomic and molecular electronic structure system, J. Comput. Chem. **14**, 1347 (1993).

[28] M. J. Frisch *et al.*, GAUSSIAN09, Gaussian, Inc., Wallingford, 2009.

[29] R. Boschi, J. N. Murrell, and W. Schmidt, Photoelectron spectra of polycyclic aromatic hydrocarbons, Faraday Discuss. Chem. Soc. **54**, 116 (1972).

[30] S. Hirata, T. J. Lee, and M. Head-Gordon, Time-dependent density functional study on the electronic excitation energies of polycyclic aromatic hydrocarbon radical cations of naphthalene, anthracene, pyrene, and perylene, J. Chem. Phys. **111**, 8904 (1999).

[31] S. Pedersen and A. H. Zewail, Femtosecond real time probing of reactions XXII Kinetic description of probe absorption fluorescence depletion and mass spectrometry, Mol. Phys. **89**, 1455 (1996).

[32] See Supplemental Material at http://link.aps.org/supplemental/10.1103/PhysRevA.91.031403 for the fitting model.

[33] T. Kiba *et al.*, Solvent-assisted intramolecular vibrational energy redistribution of S1 perylene in ketone solvents, J. Photochem. Photobiol. Chem. **178**, 201 (2006).

[34] M. A. Walker, P. Hansch, and L. D. Van Woerkom, Intensity-resolved multiphoton ionization: Circumventing spatial averaging, Phys. Rev. A **57**, R701 (1998).

[35] S. M. Hankin, D. M. Villeneuve, P. B. Corkum, and D. M. Rayner, Intense-field laser ionization rates in atoms and molecules, Phys. Rev. A **64**, 013405 (2001).

[36] M. Micciarelli *et al.*, Photophysics and photochemistry of a DNA–protein cross-linking model: A synergistic approach combining experiments and theory, J. Phys. Chem. B **118**, 4983 (2014).